Light-induced actuating nanotransducers

Tao Ding[a,b,1], Ventsislav K. Valev[a,c], Andrew R. Salmon[a,d], Chris J. Forman[d], Stoyan K. Smoukov[b], Oren A. Scherman[d], Daan Frenkel[d], and Jeremy J. Baumberg[a,1]

[a]NanoPhotonics Centre, Cavendish Laboratory, University of Cambridge, Cambridge, CB3 0HE, United Kingdom; [b]Department of Materials Science and Metallurgy, University of Cambridge, Cambridge, CB3 0FS, United Kingdom; [c]Department of Physics, University of Bath, Bath, BA2 7AY, United Kingdom; and [d]Department of Chemistry, University of Cambridge, Cambridge CB2 1EW, United Kingdom

Edited by Vinothan N. Manoharan, Harvard University, Cambridge, MA, and accepted by the Editorial Board March 30, 2016 (received for review December 9, 2015)

Nanoactuators and nanomachines have long been sought after, but key bottlenecks remain. Forces at submicrometer scales are weak and slow, control is hard to achieve, and power cannot be reliably supplied. Despite the increasing complexity of nanodevices such as DNA origami and molecular machines, rapid mechanical operations are not yet possible. Here, we bind temperature-responsive polymers to charged Au nanoparticles, storing elastic energy that can be rapidly released under light control for repeatable isotropic nanoactuation. Optically heating above a critical temperature T_c = 32 °C using plasmonic absorption of an incident laser causes the coatings to expel water and collapse within a microsecond to the nanoscale, millions of times faster than the base polymer. This triggers a controllable number of nanoparticles to tightly bind in clusters. Surprisingly, by cooling below T_c their strong van der Waals attraction is overcome as the polymer expands, exerting nanoscale forces of several nN. This large force depends on van der Waals attractions between Au cores being very large in the collapsed polymer state, setting up a tightly compressed polymer spring which can be triggered into the inflated state. Our insights lead toward rational design of diverse colloidal nanomachines.

nanoactuator | nanomachine | plasmonics | pNIPAM | colloidal

Actuators are needed to turn energy sources into physical movement. These can be for microrobotics, sensing, storage devices, smart windows and walls, or more general functional and active materials. Such artificial muscles have gained rapidly increasing interest (1, 2) leading to micropropellers (3, 4), gas jets from catalytic surfaces (5), and DNA machines (6). However, the actuation methods, delivery of energy, and forces obtained (typically 10 fN/nm^2) are limited so far (7): Magnetic fields are inconvenient to apply locally for actuation, as is >200 °C heating to actuate polymer fibers; the nanocatalysis of chemical fuels lacks controllability, whereas DNA machines rely on "fuel" DNA strands to competitively bind and operate on very slow (second) timescales. Piezoelectric-type materials used in high-end instrumentation (such as atomic force microscopy or nanopositioning stages) provide short travel but with inorganic materials that are dense, delicate, expensive, hard to fabricate, and demand high voltages (150–300 V), as is also true for electrostrictive rubbers and relaxor ferroelectrics (8, 9). Many biological systems such as *Escherichia coli* (10), cilia (11), or nematocysts (12) provide sophisticated models for nanomachines (13). Although molecular motors and artificial muscles from hydrogels (14, 15), colloids (16), or liquid crystalline elastomers (17, 18) successfully mimic such behaviors, they are very slow (on the order of seconds) and the forces generated are very small (~ pN). This is because either the energy density stored in the system is low or the energy release is inefficient.

To overcome this we design a colloidal actuating transducer system with high-energy storage (1,000 k_BT/cycle) and fast (>MHz) release mechanism. Based on gold spherical nanoparticles (Au NPs) coated with the amino-terminated polymer poly(*N*-isopropylacrylamide) (pNIPAM), this exploits the temperature-responsive coil-to-globule transition at T_c = 32 °C. Below T_c the pNIPAM is hydrophilic and swelled by water inside the gel, but when heated above T_c it becomes hydrophobic and expels all water, collapsing to a volume many times smaller. We show that in the hot collapsed state, these actuating nanotransducers (ANTs) bind to neighbors but as soon as the temperature drops below T_c they are strongly pushed apart. Optical actuation is used to directly heat the Au NPs via the plasmonic photothermal effect, allowing remote control which is reversible. The resulting nanoscale forces are several orders of magnitude larger than any produced previously, with a force per unit weight nearly a hundred times better than any motor or muscle. Together with biocompatibility, cost-effective manufacture, fast response, and energy efficiency, these deliver a step change in nanodevice performance.

Results and Discussion

Colloidal Actuators. ANTs are assembled by functionalizing 60-nm-diameter citrate-stabilized Au NPs with pNIPAM via ligand exchange above T_c (Fig. 1*A*). The amino group on the pNIPAM chains strongly binds to Au, displacing citrate, whereas the hot assembly ensures the polymers attach in their globule state, leaving enough lateral space for subsequent actuation. After initial ligand exchange, the absorption spectra of Au NPs only slightly redshifts by 1.5 nm with no aggregation (Fig. 1*B*, black to orange lines), indicating sparse coating of pNIPAM onto the Au with good stability. A resonant laser (532 nm, 5 W) irradiating the ANT solution in a cuvette for 5 min increases the NP temperature to over 35 °C (*SI Appendix*, Fig. S1), giving a dramatic redshift of the

Significance

Scientists have dreamt of nanomachines that can navigate in water, sense their environment, communicate, and respond. Various power sources and propulsion systems have been proposed but they lack speed, strength, and control. We introduce here a previously undefined paradigm for nanoactuation which is incredibly simple, but solves many problems. It is optically powered (although other modes are also possible), and potentially offers unusually large force/mass. This looks to be widely generalizable, because the actuating nanotransducers can be selectively bound to designated active sites. The concept can underpin a plethora of future designs and already we produce a dramatic optical response over large areas at high speed.

Author contributions: T.D., V.K.V., and J.J.B. designed research; T.D., V.K.V., and A.R.S. performed research; A.R.S., C.J.F., S.K.S., and O.A.S. contributed new reagents/analytic tools; T.D., V.K.V., D.F., and J.J.B. analyzed data; and T.D., V.K.V., O.A.S., D.F., and J.J.B. wrote the paper.

The authors declare no conflict of interest.

This article is a PNAS Direct Submission. V.N.M. is a guest editor invited by the Editorial Board.

Data deposition: The raw data of the figures in this paper can be found at https://www.repository.cam.ac.uk/handle/1810/254762.

[1]To whom correspondence may be addressed. Email: dt413@cam.ac.uk or jjb12@cam.ac.uk.

This article contains supporting information online at www.pnas.org/lookup/suppl/doi:10.1073/pnas.1524209113/-/DCSupplemental.

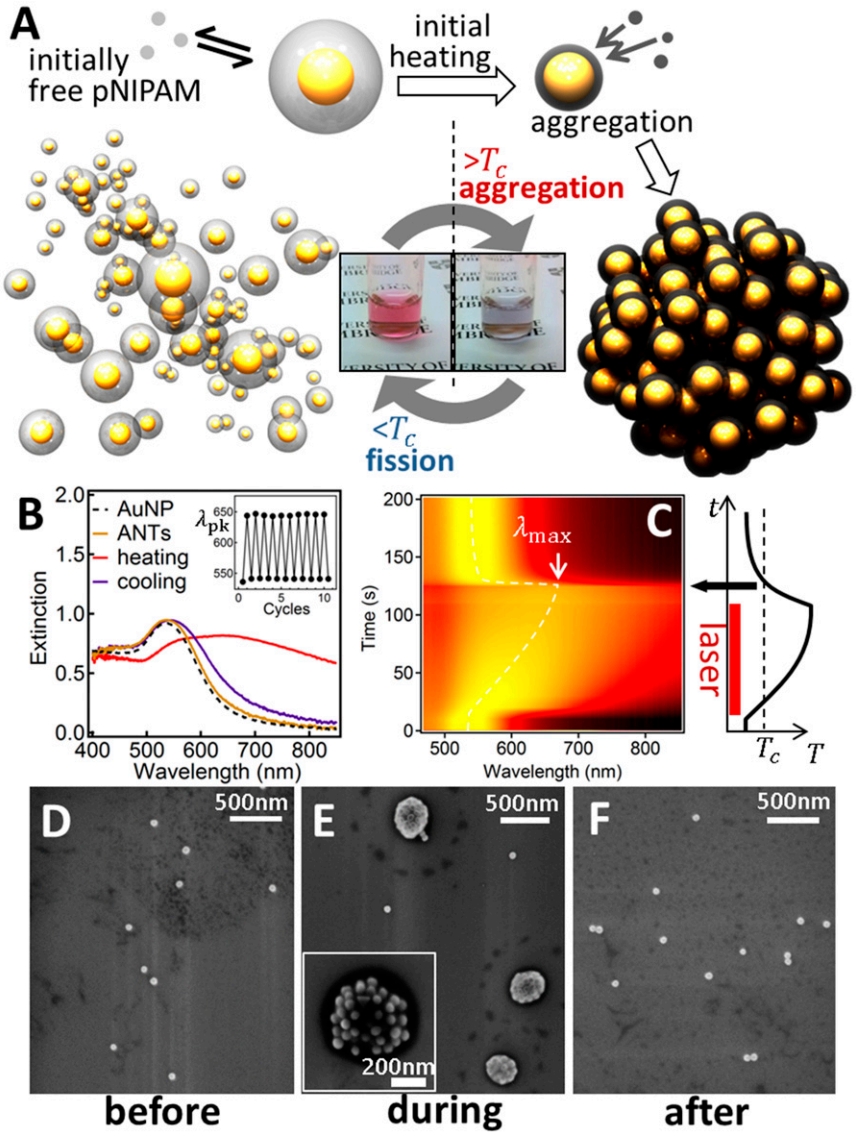

Fig. 1. Reversible assembly of ANTs. (*A*) Formation of pNIPAM-coated Au nanoparticles by mixing in solution, and heating above T_c = 32 °C to attach pNIPAM onto Au. In deflated state, NPs aggregate tightly together (blue sol). Cooling then explosively splits clusters into individual ANTs (red sol). Further heating and cooling results in reversible fission and aggregation. (*B*) Extinction spectra of Au NPs initially (black) and in 40-μM pNIPAM (orange), under laser heating (red) and cooled (purple). (*Inset*) Peak wavelength changes over successive cycles of laser heating and cooling. (*C*) Extinction spectral kinetics of Au NP–pNIPAM mixture through one cycle of laser irradiation. (*D*–*F*) SEM images of ANTs before (*D*), during (*E*), and after (*F*), irradiating with 10 W cm^{-2} for 5 min. (*D*, *Inset*) magnifies assembled ANT cluster.

extinction peak to 645 nm (red line, Fig. 1*B*). Blocking the laser rapidly cools the ANTs, and the extinction peak blueshifts back to 539 nm (purple line, Fig. 1*B*), almost recovering to its original state (at λ_{peak} = 535 nm). These spectral signatures are highly reproducible, repeating for many cycles (Fig. 1*B*, *Inset*). Similar constructs with 20–100-nm-diameter Au NPs also work successfully (*SI Appendix*, Fig. S2).

No such huge spectral shifts ($\Delta\lambda$ > 200 nm) were seen in previous attempts to use pNIPAM to reversibly tune the spacing between Au NPs for switching of plasmons (19–27). It is thus critical to clarify how pNIPAM promotes assembly and disassembly in solution, how fast the assembly can be, and what configurations are selected. Extinction spectra are recorded during irradiation every 10 s (Fig. 1*C*). The extinction peak remains stable at 536 nm in the first 30 s but increases steadily to 670 nm within 60 s. This redshift, which can reach 750 nm (see below), directly implies that the Au NPs come very close together with ever stronger coupling. Electromagnetic simulations (*SI Appendix*, Fig. S3) suggest the average gap between Au NP cores shrinks below 4 nm (agreeing well with SEMs below as well as the expected size of each globular pNIPAM, with indications also of a range of gap sizes ±1 nm), attributed to the well-known hydrophobic collapse of pNIPAM above T_c. After irradiation ceases, the plasmon resonance peak remains at ~ 670 nm for 10 s followed by an extremely rapid blueshift back to 539 nm with a time constant <1 s as soon as the pNIPAM drops below T_c. Such fast disassembly kinetics is due to the rapid swelling of pNIPAM and strong elastic forces exerted on the Au NPs.

Scanning electron microscopy (SEM) images taken at different stages confirm this assembly process (*Materials and Methods*; Fig. 1 *D*–F). Initially the Au NPs remain well dispersed (Fig. 1*D*) but above T_c, compact aggregates of Au NPs embedded in pNIPAM are found everywhere (Fig. 1*E*). Aggregates of average diameter 400 nm comprise 40 Au NPs. After cooling back down

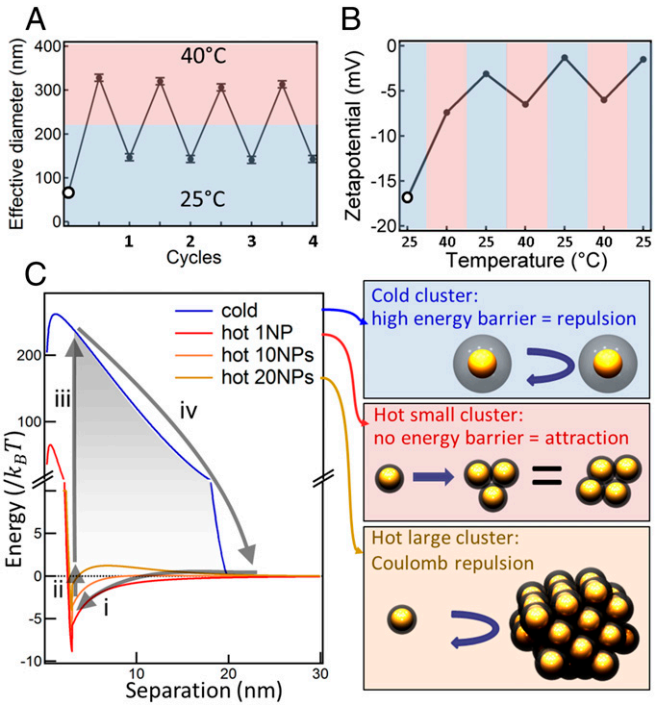

Fig. 2. Mechanism of reversible assembly. (*A*) Change of hydrodynamic size from DLS and (*B*) zeta potential, of Au–pNIPAM assembly (initial state marked ○) for four cycles of heating and cooling measured at 25 °C and 40 °C. (*C*) Potential energy when bringing extra ANT nanoparticle closer to a single cluster, in both hot (red) and cold (blue) states near T_c. In the cold state swelled ANTs bounce from each other. In the hot state, the potential energy depends on the number of NPs in the cluster as each contribute more repulsive charge (*Right*).

to room temperature, Au NPs collected in the same way show no aggregation at all (Fig. 1*F*). This laser-induced reversible shifting of plasmons occurs only in the presence of NH_2-terminated pNIPAM and when irradiating Au NPs around 532 nm (*SI Appendix*, Fig. S4). Such plasmonically enhanced laser heating of the individual NPs is well known and calibrated (28). At our dilutions, assembly only occurs when each individual Au NP (plus thin ∼10-nm water shell within the thermal diffusion length, *SI Appendix*, section S6) is heated above T_c so multiple light scattering plays little role. Irradiating silver NPs at 532 nm does not work because they lack plasmon resonances at the laser wavelength, whereas pNIPAM terminated with –COOH or without any functional group does not attach to the surface of Au NPs (*SI Appendix*, Fig. S4B) so that heating only leads to flocculation of pNIPAM (*SI Appendix*, Fig. S4C).

Reversible Clustering. Zeta potential and dynamic light-scattering (DLS) measurements (Fig. 2*A* and *B*) confirm our model of light-induced reversible tuning (Fig. 1*A*). Initially, a sparse coating of amino-terminated pNIPAM displaces some of the charged citrate originally attached to each Au NP (○). When the solution is heated above T_c (by light or heat) this pNIPAM collapses to globules and all other pNIPAM in solution quickly adds on top, yielding a thicker coat and initiating aggregation to form weakly charged clusters (Fig. 2*B*). Whereas some irreversible clustering has been observed (29, 30) based on charge compensation, here we use the balance between charge and sterics to enable reversibility. Cooling the solution back down reinflates the pNIPAM producing individual ANTs coated with pNIPAM layers 40 nm thick as estimated from their hydrodynamic diameter at 25 °C (Fig. 2*A*). These ANTs can then be repeatedly cycled from inflated (cold, isolated) to deflated (hot, aggregated) states.

Actuation Forces. Actuation works when heating and cooling the solution around T_c (only $\Delta T = 2$ °C is enough to trigger the effects here). Our quantitative model (Fig. 2*C*) includes screened Coulomb, elastic, van der Waals, solvation, and surface forces (*SI Appendix*). When cold, the pNIPAM coat is inflated with water and ANTs just bounce off each other (blue curve). When hot (red curve) the outer pNIPAM coating collapses to only a few nanometers thick, and when NPs approach close to the cluster they feel strong van der Waals attraction between the Au cores, as well as an attractive solvation force (Fig. 2 *C*, *i*). Increasing numbers of AuNPs join the cluster accumulating in the outer potential well, until the net charge (which is poorly screened by the hydrophobic collapsed pNIPAM) is enough to repel further NPs (yellow curve, Fig. 2 *C*, *ii*). After collecting a maximum number of NPs, the total cluster size thus saturates (Fig. 2*A*). This saturated cluster size is controllable through the initial charge on the Au NPs, addition of a small ethanol fraction, or salt concentration in solution, which tunes clusters from 50 to 1,000 NPs (*SI Appendix*, Fig. S5). When cooled again, the pNIPAM returns to its inflated state (Fig. 2 *C*, *iii*) but starting out highly compressed. The stored elastic energy in this state is very large, placing very large forces on the neighboring NPs and exploding the cluster back to its constituents (Fig. 2 *C*, *iv*). We estimate the potential energy stored (31) as

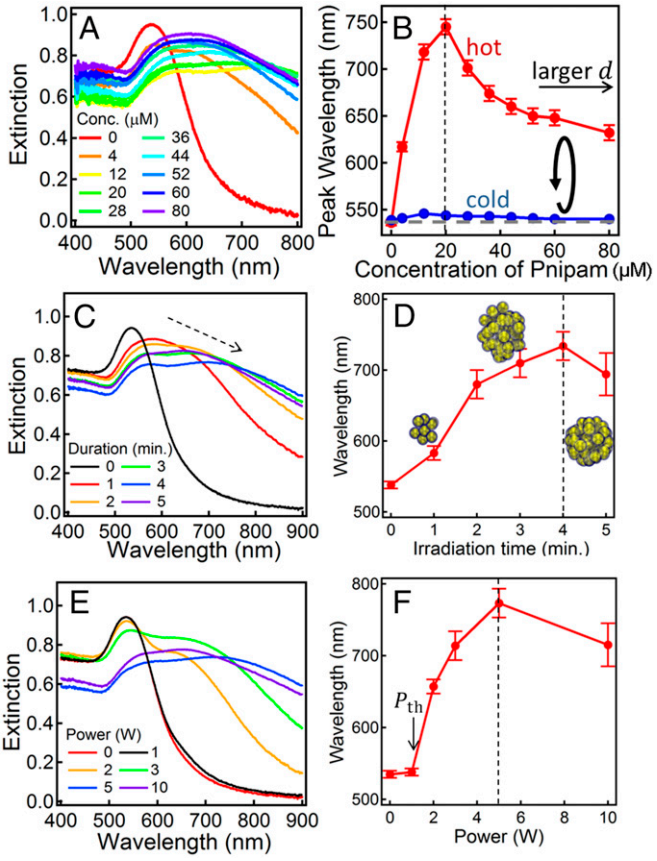

Fig. 3. ANT tunability. (*A*–*F*) Extinction spectra of Au NP–pNIPAM system at (*A* and *B*) different concentrations of pNIPAM, (*C* and *D*) different irradiation times at 5 W, and (*E* and *F*) different irradiation powers at 10 min. *B*, *D*, and *F* show corresponding extracted longitudinal coupled plasmon mode wavelengths from *A*, *C*, and *E*.

$$U = 0.1\, Y_c \sqrt{R}\, t^{5/2}, \quad [1]$$

where Y_c = 1.8 MPa is the Young's modulus in the cold state of pNIPAM, R is the radius of the Au NP, and t is the thickness of the pNIPAM layer when cold. This potential energy from individual pairs of ANTs can reach 200–2,500 k_BT for each cycle around this compression–expansion curve (shaded, Fig. 2*C*), depending on their size and coating. The resulting expansion force

$$F = 0.1\, Y_c \sqrt{R}\, t^{3/2}, \quad [2]$$

is ∼5 nN for R = 30 nm, t = 40 nm. Because typical Brownian forces in solution are 1 pN, 4 orders of magnitude less, this is what forces the clusters apart into composite nanoparticles.

Surveying macroscale to nanoscale actuators (32) shows forces scale with mass m, as $\log_{10} F \simeq 3 + (2/3)\log_{10} m$, predicting maximum 1-nN forces from our NPs. The origin for the near-100-fold improvement here depends on van der Waals attractions between Au cores being very large in the collapsed pNIPAM state, setting up a tightly compressed pNIPAM spring which can be triggered into the inflated state. These forces thus compare very favorably with typical forces/weight from current molecular motors (rotaxanes and kinesins), muscles, as well as mechanical and piezoelectric devices, and function much like a nanonematocyst (33). Direct measurement of the force impulse given by ANTs is nontrivial because the expansion process is so fast (see below), but we resolve large force spikes when the expanding pNIPAM hits the bottom of a suspended AFM tip (*SI Appendix*, Fig. S9).

Optical Actuation. Light-triggered actuation allows tuning of the nanoassembly by varying pNIPAM concentration, laser irradiation time, and power (Fig. 3). The initial pNIPAM concentration controls the surface charge of the Au NPs (*SI Appendix*, Fig. S10), and is crucial in determining the cluster saturation size. For pNIPAM concentrations below 20 μM, the plasmon resonance peak can redshift to 745 nm, but this redshift decreases at higher concentration (Fig. 3 *A* and *B*). With excess pNIPAM the coating thickness increases, spacing the Au NP cores further apart within the cluster and decreasing the maximum redshift. In all cases, the ANTs recover to their initial state around 535 nm (blue, Fig. 3*B* and *SI Appendix*, Fig. S11).

Irradiation times influence the temperature of the ANTs (*SI Appendix*, Fig. S1), changing the kinetics of pNIPAM assembly onto Au NPs (Fig. 3 *C* and *D*). As irradiation times increase, the clusters grow, limited by their charge balance and diffusion (*SI Appendix*, Fig. S15). Similar effects are seen with increasing laser powers providing they exceed the $P_{th} \sim 1\text{-Wcm}^{-2}$ threshold needed to trigger the thermal transition (Fig. 3 *E* and *F*). Small blueshifts at the highest powers or longest times can arise with rearrangement of AuNP clusters from nonspherical aggregates into more compact arrangements. Once the ANTs have formed however, in all cases the extinction spectra recover to the initial wavelength after cooling (*SI Appendix*, Fig. S12), showing laser irradiation does not cause irreversible aggregation, due to the strong elastic repulsion between ANTs.

Actuator Performance. This colloidal actuator enables remote light control of nanodevices through reversible expansion between AuNPs. Fabrication of the actuator nanoparticles on a large scale, and their operational mechanism, are both simple. They are compatible with aqueous environments and work at room temperature, with T_c tunable in many ways (such as pH or ethanol fraction, *SI Appendix*, Fig. S13). Whereas the ANT expansions are currently isotropic, more directional actuation performance can develop from appropriate integration into geometrically defined devices. For a simple demonstration, we encapsulate individual ANT clusters on a substrate with a 70-nm-thick agarose film (Fig. 4 *A* and *B* and *SI Appendix*, Figs. S6 and S7). By monitoring its color changes and spectral shifts in the dark-field scattering as the temperature is cycled (Fig. 4 *C* and *E*), we can optically track the actuation of the ANT cluster. Estimates of the heating and cooling rates (*SI Appendix*) suggest subnanosecond switching is possible, thus enabling up to GHz-rate cycling and yielding available powers ∼ nW per nanoparticle. Optical triggering (*SI Appendix*) of single agarose-encapsulated clusters indeed shows <2 μs (video rate) switching (Fig. 4*D*), limited by our system response (*SI Appendix*, Fig. S14), which is already 10^6 times faster than typical pNIPAM switching (14). We note that little is yet known about the switching rates of single pNIPAM molecules, although hydrogen bonding network changes are extremely fast. Estimates for the individual ANT switching (*SI Appendix*) show 1–10-fJ energies are possible.

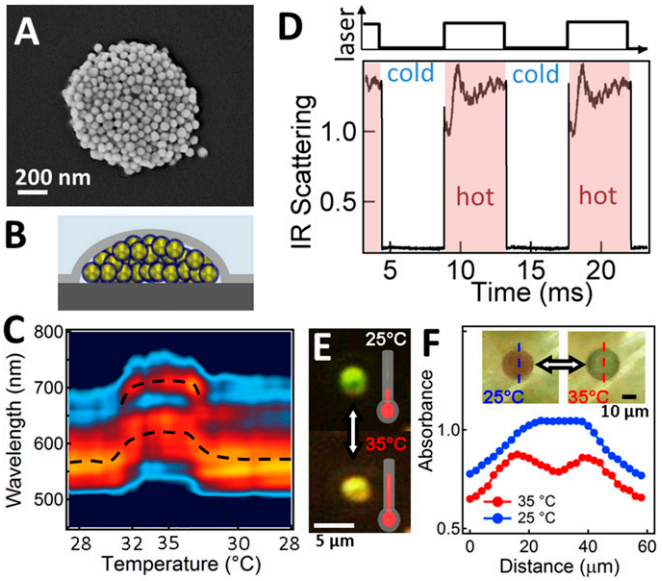

Fig. 4. Dynamics of nanomachines. (*A*) SEM of agarose-encapsulated ANT cluster on Si, with (*B*) schematic. (*C*) Scattering spectra of the agarose-encapsulated ANT cluster on Si when cycling the temperature between 28 °C and 35 °C, with (*D*) scattering dynamics (integrated from 700 to 900 nm) when modulated by 0.5-mW 635-nm laser (*Top*), and (*E*) dark-field images. (*F*) Absorbance profile across a single microdroplet (*Inset*, images) containing pNIPAM and 60-nm AuNPs, when thermally cycled to drive the ANTs onto and off the oil/water interface.

Upon cooling, the agarose is found to be forced up around the cluster edges by the swelling ANTs, which require forces ∼ 100 nN (*SI Appendix*). These estimates for strong forces are corroborated by observing ANTs in aqueous microdroplets within oil. Whereas surface forces normally permanently tether >10-nm Au NPs to water/oil interfaces, we observe completely reversible switching with the 60-nm Au NPs pushed back away from the interface on each cooling (Fig. 4*F* and *SI Appendix*, Fig. S8).

Van der Waals forces are crucial in providing sufficient attractive force in the collapsed pNIPAM state to bind NPs, while being not too strong to prevent them being thrust apart when switching the pNIPAM to the inflated state. The high optical cross-section of plasmonic Au NP cores enhances the local energy absorbed from the incident light, reducing the total power needed to switch the pNIPAM surrounding each NP. Whereas Au cores are thus ideal, van der Waals forces between other metallic cores also work. Critical for reversibility here is the charging limit on cluster size, without which clusters grow large and insoluble. Such nanoactuators are expected to prove of great utility in on-demand remotely controlled, fully

reversible dynamic assembly, for nanomachines such as DNA origami (*SI Appendix*, Fig. S16), for overcoming the problematic surface tension in microdroplets (Fig. 4*F* and *SI Appendix*, Fig. S9) and microelectronic mechanical devices, for optically controlled microfluidic pumps and valves, as well as for wallpaper-scale optics such as nonfading large-area photochromics for buildings (color changes in Fig. 1*A*). Although we demonstrate here reversible expansion and contraction, adapting this for nanomachinery requires reconfiguring the isotropic-into directional-forces, for instance by nanoconfinement, attachment to scaffolds, or nonisotropic pNIPAM coating.

Materials and Methods

Methods and any associated references are available in the *SI Appendix*. The raw data of the figures in this paper can be found at https://www.repository.cam.ac.uk/handle/1810/254762.

ACKNOWLEDGMENTS. We thank Edward Booker for help with temperature measurements; Rohit Chikkaraddy for simulations; and Elisa Hemmig, Vivek Thacker, and Ulrich Keyser for providing DNA origami samples. This research is supported by UK Engineering and Physical Sciences Research Council Grants EP/G060649/1 and EP/L027151/1, and ERC Grants LINASS 320503 and EMATTER 280078. V.K.V. acknowledges support from The Royal Society through the University Research Fellowships.

1. Shahinpoor M, Kim KJ, Mojarrad M (2007) *Artificial Muscles: Applications of Advanced Polymeric Nanocomposites* (Taylor & Francis, New York).
2. Haines CS, et al. (2014) Artificial muscles from fishing line and sewing thread. *Science* 343(6173):868–872.
3. Ghosh A, Fischer P (2009) Controlled propulsion of artificial magnetic nanostructured propellers. *Nano Lett* 9(6):2243–2245.
4. Dreyfus R, et al. (2005) Microscopic artificial swimmers. *Nature* 437(7060):862–865.
5. Ebbens SJ, Howse JR (2010) In pursuit of propulsion at the nanoscale. *Soft Matter* 6(4): 726–738.
6. Bath J, Turberfield AJ (2007) DNA nanomachines. *Nat Nanotechnol* 2(5):275–284.
7. Ozin GA, Manners I, Fournier-Bidoz S, Arsenault A (2005) Dream nanomachines. *Adv Mater* 17(24):3011–3018.
8. Pelrine R, Kornbluh R, Pei Q, Joseph J (2000) High-speed electrically actuated elastomers with strain greater than 100%. *Science* 287(5454):836–839.
9. Carpi F, Bauer S, De Rossi D (2010) Materials science. Stretching dielectric elastomer performance. *Science* 330(6012):1759–1761.
10. Whitesides GM (2001) The once and future nanomachine. *Sci Am* 285(3):78–83.
11. Sanchez T, Welch D, Nicastro D, Dogic Z (2011) Cilia-like beating of active microtubule bundles. *Science* 333(6041):456–459.
12. Weber J (1989) Nematocysts (stinging capsules of Cnidaria) as Donnan-potential-dominated osmotic systems. *Eur J Biochem* 184(2):465–476.
13. Schliwa M, Woehlke G (2003) Molecular motors. *Nature* 422(6933):759–765.
14. Xia L-W, et al. (2013) Nano-structured smart hydrogels with rapid response and high elasticity. *Nat Commun* 4:2226.
15. Zarzar LD, Aizenberg J (2014) Stimuli-responsive chemomechanical actuation: A hybrid materials approach. *Acc Chem Res* 47(2):530–539.
16. Shah AA, Schultz B, Zhang W, Glotzer SC, Solomon MJ (2015) Actuation of shape-memory colloidal fibres of Janus ellipsoids. *Nat Mater* 14(1):117–124.
17. Ohm C, Brehmer M, Zentel R (2010) Liquid crystalline elastomers as actuators and sensors. *Adv Mater* 22(31):3366–3387.
18. Pei Z, et al. (2014) Mouldable liquid-crystalline elastomer actuators with exchangeable covalent bonds. *Nat Mater* 13(1):36–41.
19. Wang C, Flynn NT, Langer R (2004) Controlled structure and properties of thermoresponsive nanoparticle–hydrogel composites. *Adv Mater* 16(13):1074–1079.
20. Contreras-Cáceres R, et al. (2009) Au@pNIPAM thermosensitive nanostructures: Control over shell cross-linking, overall dimensions, and core growth. *Adv Funct Mater* 19(19):3070–3076.
21. Zhu M-Q, Wang L-Q, Exarhos GJ, Li ADQ (2004) Thermosensitive gold nanoparticles. *J Am Chem Soc* 126(9):2656–2657.
22. Contreras-Cáceres R, et al. (2008) Encapsulation and growth of gold nanoparticles in thermoresponsive microgels. *Adv Mater* 20(9):1666–1670.
23. Fava D, Winnik MA, Kumacheva E (2009) Photothermally-triggered self-assembly of gold nanorods. *Chem Commun (Camb)* (18):2571–2573.
24. Karg M, Pastoriza-Santos I, Pérez-Juste J, Hellweg T, Liz-Marzán LM (2007) Nanorod-coated PNIPAM microgels: Thermoresponsive optical properties. *Small* 3(7): 1222–1229.
25. Han H, Lee JY, Lu X (2013) Thermoresponsive nanoparticles + plasmonic nanoparticles = photoresponsive heterodimers: Facile synthesis and sunlight-induced reversible clustering. *Chem Commun (Camb)* 49(55):6122–6124.
26. Karg M, Hellweg T, Mulvaney P (2011) Self-assembly of tunable nanocrystal superlattices using poly-(NIPAM) spacers. *Adv Funct Mater* 21(24):4668–4676.
27. Honda M, Saito Y, Smith NI, Fujita K, Kawata S (2011) Nanoscale heating of laser irradiated single gold nanoparticles in liquid. *Opt Express* 19(13):12375–12383.
28. Govorov AO, Richardson HH (2007) Generating heat with metal nanoparticles. *Nano Today* 2(1):30–38.
29. Stradner A, et al. (2004) Equilibrium cluster formation in concentrated protein solutions and colloids. *Nature* 432(7016):492–495.
30. Xia Y, et al. (2011) Self-assembly of self-limiting monodisperse supraparticles from polydisperse nanoparticles. *Nat Nanotechnol* 6(9):580–587.
31. Lau AWC, Raphaël MPE, Léger L (2002) Spreading of latex particles on a substrate. *Europhys Lett* 60(5):171.
32. Marden JH, Allen LR (2002) Molecules, muscles, and machines: Universal performance characteristics of motors. *Proc Natl Acad Sci USA* 99(7):4161–4166.
33. Nüchter T, Benoit M, Engel U, Ozbek S, Holstein TW (2006) Nanosecond-scale kinetics of nematocyst discharge. *Curr Biol* 16(9):R316–R318.